NIH Public Access
Author Manuscript
Mol Ther. Author manuscript; available in PMC 2008 December 1.

Published in final edited form as:
Mol Ther. 2008 June ; 16(6): 1129–1137. doi:10.1038/mt.2008.64.

Adult Bone Marrow-Derived Cells Do Not Acquire Functional Attributes of Cardiomyocytes Upon Transplantation Into Peri-Infarct Myocardium

John A. Scherschel[1,2], **Mark H. Soonpaa**[1,2], **Edward F. Srour**[1,3,4], **Loren J. Field**[1,2], and **Michael Rubart**[1]

1*Department of Pediatrics, Division of Cardiology, Wells Center for Pediatric Research, 1044 West Walnut Street, Indianapolis, IN 46202*

2*Department of Medicine, Division of Cardiology, Krannert Institute of Cardiology, Indiana University School of Medicine, Indianapolis, IN 46202*

3*Department of Medicine, Division of Hematology/Oncology, Indiana University School of Medicine, Indianapolis, IN 46202*

4*Department of Microbiology/Immunology, Indiana University School of Medicine, Indianapolis, IN 46202*

Abstract

The cardiomyogenic potential of adult bone marrow (BM) cells following their direct transplantation into the ischemically injured heart remains controversial. Here, we investigated the ability of transplanted BM cells to develop intracellular calcium ($[Ca^{2+}]_i$) transients in response to membrane depolarization *in situ*. Low-density mononuclear (LDM) BM cells, c-kit-enriched (c-kit^{enr}) BM cells, and highly enriched lin$^-$ c-kit$^+$ BM cells, were obtained from adult transgenic mice ubiquitously expressing enhanced green fluorescent protein (EGFP) and injected into peri-infarct myocardium of non-transgenic mice. After 9–10 days the hearts were harvested, perfused in Langendorff mode, loaded with the calcium-sensitive fluorophore rhod-2, and subjected to two-photon laser scanning fluorescence microscopy to monitor action potential-induced $[Ca^{2+}]_i$ transients in EGFP-expressing donor-derived cells and non-expressing host cardiomyocytes. Whereas spontaneous and electrically evoked $[Ca^{2+}]_i$ transients were found to occur synchronously in host cardiomyocytes along the graft-host border and in areas remote from the infarct, they were absent in all of the more than 3,000 imaged BM-derived cells that were located in clusters throughout the infarct scar or peri-infarct zone. We conclude that engrafted BM-derived cells lack attributes of functioning cardiomyocytes, calling into question the concept that adult BM cells can give rise to substantive cardiomyocyte regeneration within the infarcted heart.

Introduction

Conflicting data exist as to the ability of adult bone marrow (BM) cells to give rise to cardiomyocytes within the injured heart.[1] The possibility of cardiomyocyte formation by adult BM-derived stem cells was initially demonstrated in a study by Bittner et al. [2], who observed dystrophin-expressing cardiomyocytes in mdx mice following BM reconstitution with wild-type donor cells. Subsequently, Jackson and co-workers [3] induced myocardial ischemia/reperfusion injury in mice following BM reconstitution with so-called side population cells

Correspondence should be addressed to M. R. (mrubartv@iupui.edu), Wells Center for Pediatric Research, 1044 West Walnut Street, Indianapolis, IN 46202, USA, Phone: 317-278-1538, Fax: 317-278-5413.

NIH-PA Author Manuscript
NIH-PA Author Manuscript
NIH-PA Author Manuscript

NIH-PA Author Manuscript

NIH-PA Author Manuscript

NIH-PA Author Manuscript

that were genetically engineered to express β-galactosidase. Donor-cell derived cardiomyocytes were detected in the peri-infarct zone, albeit at a very low prevalence (0.02%). A study by Xaymardan et al. [4] showed that a small percentage of fluorescently labeled unfractionated BM cells obtained from adult rats can acquire a cardiomyocyte phenotype in an infarct transplantation model. Similarly, fluorescently tagged BM mononuclear cells from patients with previous myocardial infarction were shown to transdifferentiate into cardiomyocytes when seeded on cyroinjured mouse ventricle in culture.[5]

A limited number of studies reported extensive myocardial regeneration from BM-derived cells within the infarcted heart.[6,7] In these latter studies, female mice were subjected to permanent coronary artery ligation and c-kit-positive BM cells from adult male transgenic mice ubiquitously expressing enhanced green fluorescent protein (EGFP) were directly injected into the viable peri-infarct region. *De novo* formation of donor cell-derived cardiomyocytes was assessed by co-staining for cardiomyocyte-specific markers plus Y chromosome or EGFP. By this approach, it was demonstrated that transplanted BM cells could give rise to millions of new cardiomyocytes by 9 days after intracardiac injection, resulting in partial replacement of the scar with functioning muscle. The concomitant improvement of left ventricular contractility lead the authors to suggest that *de novo* cardiomyocytes became electromechanically integrated and were thus capable of directly contributing to the overall pump function of the injured heart.

Numerous other studies have failed to observe cardiomyogenic differentiation from adult BM-derived donor cells. For example, Balsam and co-workers [8] demonstrated that purified populations of adult hematopoetic stem cells (HSCs) obtained from transgenic mice widely expressing EGFP transiently engrafted within the infarcted myocardium, but did not express cardiac tissue-specific markers. Rather, most of the donor-derived cells expressed the pan-hematopoetic marker CD45 and the myeloid marker Gr-1. Nygren and co-workers [9] did not observe cardiomyogenic transformation of unfractionated BM cells or c-kit$^+$ enriched HSCs following engraftment within the infarcted mouse myocardium, as evidenced by the absence of cardiomyocyte-specific immune reactivity in the donor cells. Finally, Murry et al. [10] utilized cardiomyocyte-restricted transgenes (expressing either beta-galactosidase or EGFP under the regulation of the alpha-cardiac Myosin Heavy Chain promoter) as well as a ubiquitously expressed EGFP reporter transgene (in conjunction with histochemical analyses) to track the fate of two purified populations of BM-derived HSCs (lin$^-$ c-kit$^+$ and lin$^-$ c-kit$^+$ sca-1$^+$ cells) following their transplantation into injured hearts. Although donor cells engrafted in the damaged muscle, no transdifferentiation events were detected as evidenced by the lack of expression of a cardiomyocyte-restricted reporter transgene, as well as the absence of cardiomyocyte-specific immune reactivity in the donor cells.[10]

Collectively, regeneration of cardiomyocytes from adult BM-derived cells within the injured heart remains highly controversial, despite the use of seemingly identical donor cells and experimental conditions. Here we elected to use an assay which relied on examination of function, rather than potentially subjective immune histologic endpoints, to examine the regenerative potential of adult BM-derived cells in the infarcted heart. Specifically, we systematically probed the ability of engrafted BM-derived cells to develop intracellular calcium ($[Ca^{2+}]_i$) transients in response to membrane depolarization within the intact heart, using a previously developed two-photon laser scanning microscopy (TPLSM)-based imaging technique.[11,12] A side-by-side comparison of low-density mononuclear (LDM) BM cells, c-kit-enriched (c-kit^{enr}) BM cells, and highly enriched hematopoetic stem cells (lin$^-$ c-kit$^+$ BM cells), obtained from adult transgenic mice ubiquitously expressing EGFP, was performed. We demonstrate that all donor cell types were efficiently engrafted in the infarcted tissue of non-transgenic recipient hearts at 9 days following cell injection. However, while spontaneous and electrical stimulation-induced $[Ca^{2+}]_i$ transients were observed to occur synchronously in host cardiomyocytes along the graft-host border, they were absent in all of the more than 3,000

NIH-PA Author Manuscript

NIH-PA Author Manuscript

NIH-PA Author Manuscript

imaged BM-derived cells that were located in clusters within the infarct scar or border zone. These results indicate that engrafted BM-derived cells lack fundamental attributes of functioning cardiomyocytes and further call into question the concept that adult BM cells can give rise to substantive cardiomyocyte regeneration within the infarcted heart.

Results

Donor cell preparation

ACT-EGFP mice were used to isolate donor BM cells. These mice express EGFP under the control of the chicken β-actin promoter.[13] In control experiments, a comparison of 10-μm sections obtained from adult *ACT-EGFP* and wild-type hearts under epifluorescence illumination demonstrated that all cardiomyocytes in the transgenic hearts expressed EGFP throughout the cytoplasm and nuclei (Fig. 1). Kinetics of electrically evoked $[Ca^{2+}]_i$ transients in adult *ACT-EGFP* hearts were indistinguishable from those in wild type hearts (not shown). From these observations we expect any BM-derived cardiomyocytes from *ACT-EGFP* mice to stably express EGFP, and to function normally.

Three different donor BM cell populations were studied, namely low-density mononuclear (LDM) BM cells, c-kit-enriched (c-kit^{enr}) BM cells, and highly enriched lineage negative (lin$^-$) c-kit$^+$ BM cells. LDM BM cells were isolated using a density centrifugation protocol as published previously.[9] c-kit^{enr} BM cells were isolated using magnet-activated cell sorting. Flow cytometry analyses of the c-kit^{enr} BM cells demonstrated that the percentage of c-kit-positive cells in the eluted (i.e., labeled) fraction from the magnetic column was ca. 5- to 6-fold larger than that in the eluent (i.e. unlabeled) fraction (Fig. 2A). The c-kit^{enr} BM cell population was further assayed for the expression of EGFP and a variety of surface antigens. Prior to enrichment, 35% (dotted area in Fig. 2B) of the cells in the initial LDM BM preparation were EGFP positive (Fig. 2C). We confirmed the percentage of EGFP-expressing cells in additional epifluorescence analyses. Our number is in good agreement with previous studies using EGFP reporter transgenes to track the cardiomyogenic potential of marrow-derived cells.[7,14] c-kit^{enr} BM cells were 45% negative for a cocktail of antibodies recognizing mature hematopoetic cells, including lymphocytes, monocytes, granulocytes, neutrophiles, and erythrocytes (Fig. 2D). Markers for hematopoetic stem and progenitor cells (CD34, sca-1, flk-1) were present in 4% (flk-1) to 21 % (sca-1) of the c-kit^{enr} BM cell population (Fig. 2E–G). Restricting the flow cytometry analysis to the subfraction of EGFP-positive cells within the c-kit^{enr} BM cell population did not alter the expression profile of surface antigens (see Supplementary Fig. 1), suggesting that the presence of the fluorescent protein does not impart negative or positive selections on BM subpopulations. Highly enriched lin$^-$ c-kit$^+$ BM cells were prepared by first removing cells expressing hematopoetic lineage markers via magnetic immunobead subtraction.[15] This lin$^-$ fraction was then reacted with an anti-c-kit monoclonal antibody and separated by FACS into c-kit$^+$ and c-kit$^-$ cells (Fig. 2H). Lin$^-$ cells that showed c-kit expression levels 2-fold to 100-fold higher than EGFP$^-$/c-kit$^-$ cells were used for intracardiac transplantation (only EGFP-expressing cells were used).

ACT-EGFP BM-derived cells stably engraft infarcted myocardium

The peri-infarct regions of non-transgenic hearts were injected with 100,000 LDM, c-kit^{enr} or lin$^-$ c-kit$^+$ BM cells. The hearts were subsequently harvested and processed to monitor scar formation and donor cell viability, using Sirius Red/Fast Green histochemical staining and a chromogenic anti-EGFP immune reactivity assay, respectively. Analysis was performed at 9 to 10 days post-engraftment, as previous studies had suggested extensive cardiomyocyte regeneration from lin$^-$ c-kit$^+$ BM cells within this time period.[6,7,16] Fig. 3 shows representative examples of grafts generated with each cell type. In accordance with previous observations,[6,7,8,9,10,16] we found high levels of EGFP$^+$ cells that were primarily located in

NIH-PA Author Manuscript

NIH-PA Author Manuscript

NIH-PA Author Manuscript

clusters throughout the infarcted tissue and in the bordering peri-infarct zone rather than in the viable myocardium. Thus, all three BM-derived donor cell types survived and efficiently engrafted infarcted myocardium.

It had been reported previously that green autofluorescence can be mistaken as EGFP fluorescence in the ischemically injured heart under epifluorescence illumination.[17] TPLSM imaging of peri-infarct regions in Langendorff-perfused mouse hearts similarly revealed strongly autofluorescent structures. They could however be reliably distinguished from EGFP fluorescence on the basis of their distinct emission profiles under the vital imaging conditions used in this study (for details, see Supplementary Data and Supplemenrary Fig. 2).

Engrafted donor-derived cells lack electrically evoked $[Ca^{2+}]_i$ transients

We next investigated the functional fate of *ACT-EGFP* BM-derived cells following transplantation into peri-infarct regions. Hearts receiving LDM BM cells were examined first. Hearts were harvested 9 or 10 days following BM cell injection, loaded with rhod-2 (a calcium-sensitive fluorescent dye) and subjected to TPLSM imaging. Imaging was initially performed along the graft/host border as the presence of $[Ca^{2+}]_i$ transients in host cardiomyocytes within the same microscopic field provided a good positive control. A representative frame-mode image obtained during remote point stimulation at 4 Hz is shown in Fig. 4A. A cluster of small (< 10 μm diameter), round donor-derived cells, readily identifiable by virtue of their EGFP fluorescence, were present adjacent to the peri-infarct border zone of the host myocardium. Host cardiomyocytes located on either side of the BM cell graft exhibited periodic increases in rhod-2 fluorescence (denoted by asterisks), reflecting cyclic increases in intracellular free calcium triggered by propagated action potentials. The calcium responses in these cells appear to be in synchrony and at the same frequency as remote stimulation, indicating that they are functionally coupled to the remote myocardium outside the peri-infarct region. In contrast, no $[Ca^{2+}]_i$ transients were detectable in the cluster of EGFP-expressing donor-derived cells.

We also obtained line-scan images from the graft/host border by repeatedly scanning at a high rate (500 Hz) along the white line in panel A of Fig. 4 during remote electrical stimulation at 4 Hz. The scan line traversed a host cardiomyocyte, a juxtaposed capillary, and a small donor-derived cell. The line scans were then stacked such that the y-axis represents time and the x-axis represents distance (Fig. 4B). Spatially averaged traces for the red and green fluorescence signal were then generated from the line-scan data (Fig. 4C). These traces confirm the presence of action potential-evoked calcium responses in the host cardiomyocytes, and absence of calcium responses in the neighboring LDM BM-derived cells. A series of *X, Y* scans taken at 4-μm *z*-steps along the graft/host border during continuous electrical point stimulation at 4 Hz similarly did not reveal calcium responses in the cluster of donor-derived cells (Fig. 4D).

To exclude the possibility that the absence of spontaneous and remote stimulation-evoked $[Ca^{2+}]_i$ transients in donor-derived cells results from a lack of electrical coupling between donor and host cells (rather than from an intrinsic inability to raise cytosolic calcium in response to membrane depolarization), we also monitored changes in $[Ca^{2+}]_i$ during electrical field stimulation (100 V, 2 ms, 3 Hz). Under these conditions, development of $[Ca^{2+}]_i$ transients is no longer dependent on intercellular action potential propagation. Electrical field stimulation readily evoked $[Ca^{2+}]_i$ transients in host cardiomyocytes at sites remote from the graft as well as in areas bordering donor cell clusters, but not in donor-derived cells within the clusters. Collectively, these data indicate that engrafted LDM BM-derived cells within the infarcted tissue lack the ability to transiently raise cytosolic calcium in response to electrical membrane excitation. Similarly, no $[Ca^{2+}]_i$ transients were inducible in BM-derived cell clusters in the center of the scar during spontaneous sinus rhythm, remote electrical point stimulation, or electrical field stimulation. A total of > 300 LDM BM-derived cells imaged and distributed among 8 animals were shown to lack spontaneous or electrically evoked $[Ca^{2+}]_i$ transients.

NIH-PA Author Manuscript

NIH-PA Author Manuscript

NIH-PA Author Manuscript

We next examined the functional fate of c-kit^{enr} and lin^{-} c-kit^{+} BM cells following their direct injection into peri-infarct regions. Representative TPLSM images obtained from hearts 9 days after transplantation of either donor cell type are shown Fig. 5 and Fig. 6. Frame-mode and line-scan mode images revealed synchronous and periodic increases in rhod-2 fluorescence in host cardiomyocytes at the graft/host border during electrical point stimulation at 4 Hz, but not in donor-derived cell clusters, which in many cases appeared to be in physical contact with functioning host myocytes (see panels A in Fig. 5 and Fig. 6). Line scan data (panels B in Fig. 5 and Fig. 6) was used to generate spatially averaged traces for the green and red fluorescent signals (panels C in Fig. 5 and Fig. 6), which confirmed the presence and absence, respectively, of action potential-evoked $[Ca^{2+}]_i$ transients in host cardiomyocytes and donor-derived cells. Electrical field stimulation also failed to evoke cytosolic calcium transients in these donor-derived cell populations. Moreover, we did not detect spontaneous or electrically evoked calcium responses in donor-derived cells located within the infarct scar remote from functioning host cardiomyocytes. Identical results were obtained in a total of >1,700 and >1,300 donor-derived cells following transplantation of c-kit^{enr} and lin^{-} kit^{+} BM cells, respectively. These cells were distributed among 10 independent animals per group. Thus, our results indicate that the clustered EGFP-expressing cells, whether they were derived from LDM, c-kit^{enr}, or lin^{-} c-kit^{+} BM cells, lack the ability to develop cytosolic calcium transients in response to membrane depolarization, and consequently do not function as cardiomyocytes following direct transplantation into ischemically injured heart muscle.

Donor BM cells express hematopoetic lineage markers

Further evidence that the transplanted BM cells do not adopt a cardiomyocyte phenotype was obtained by immunohistological analyses. At 9 days after transplantation, immune staining revealed that clusters of EGFP-expressing cells, irrespective of the transplanted donor cell type, engrafted the infarct scar or infarct border zone (Fig. 7A, D and G), and expressed the pan-hematopoetic cell surface antigen CD45 (Fig. 7B, E and H), suggesting differentiation into mature hematopoetic cells. Morphologically, CD45- and EGFP- double positive cells predominately exhibited a round shape, compatible with a hematopoetic phenotype (Fig. 7C, F and I). Occasionally, they had a more elongated shape reminiscent of the CD-45-positive fibroblast population recently described by Haudek and co-workers [18] (Fig. 7J and K). Moreover, immunestaining with an anti-α-actinin antibody revealed that no EGFP expressing cell exhibited sarcomeric structure. In contrast, sarcomeric structure was readily apparent in host cardiomyocytes (Fig. 7L).

Limitations of the TPLSM imaging system

Accurate discrimination of donor cell rhod-2 fluorescence intensities from host cell fluorescence is crucial to unambiguously determine the functional state of individual donor cell-derived, EGFP-expressing cells *in situ*. All of the results presented above focused on the analysis of clusters of donor-derived cells, where interference from host cell rhod-2 fluorescence is not problematic. However, it was not clear if the TPLSM system has sufficient resolution on the *z*-axis to discriminate between donor vs. host cell rhod-2 fluorescence when imaging isolated donor cells closely juxtaposed to host cardiomyocytes, particularly given the small size of the engrafted EGFP-expressing BM-derived cells. Preliminary control experiments to address this caveat entailed image analysis of a non-engrafted, rhod-2 loaded, isolated perfused heart. Serial optical sections were recorded at 2.0-μm axial intervals across a bifurcated capillary during continuous electrical point stimulation at a rate of 4 Hz. Action potential-induced rhod-2 transients were visible as ripple-like wave fronts which encompass the entire width of the field of view, even when the focal plane is moved into the capillary lumen (Fig. 8A, arrows). *X, Z* reconstructions of the same capillary during continuous electrical stimulation confirmed the apparent presence of rhod-2 transients within the capillary lumen (Fig. 8B, arrows). Identical observations were made in three more hearts. These findings

NIH-PA Author Manuscript

NIH-PA Author Manuscript

NIH-PA Author Manuscript

indicate a degradation of spatial resolution at depth in living cardiac tissue under our imaging conditions. Measurements of the three-dimensional fluorescence profile of 1-μm fluorescent spheres following intracoronary injection into Langendorff-perfused heart revealed that a marked axial, but not lateral, broadening of the two-photon excitation volume underlies the decline of spatial resolution at depth (see Supplementary Data and Supplementary Fig. 3). Consequently, the apparent occurrence of rhod-2 transients within the capillary lumen (Fig. 8A and B) reflects contamination from rhod-2 signals originating in cardiomyocytes both below and above the imaged capillary. Because we found that the axial dimension of a perfusate-filled capillary lumen in a Langendorff-perfused mouse heart is typically 8 – 10 μm (measured from *z*-stacks taken across capillaries as shown in Fig. 8), we estimate that rhod-2 signals sampled from voxels located within at least a 5-μm axial distance from a donor-host cell interface will represent variable contributions from both cell types. Given this, and given the dimensions of the engrafted BM-derived EGFP expressing cells, the TPLSM imaging system cannot be used to screen for the presence of $[Ca^{2+}]_i$ transients in isolated donor cells when they are closely juxtaposed to host cardiomyocytes on the *z*-axis.

Discussion

The data presented here confirm the ability of adult LDM, c-kit^{enr}, and lin$^-$ c-kit$^+$ BM cells to efficiently engraft when directly injected into hearts of mice subjected to acute coronary artery ligation. In accordance with previous observations,[6,7,8,9,10,16] we found that the vast preponderance of donor-derived cells were located in clusters throughout the infarcted tissue and the bordering peri-infarct zone 9 days after artery occlusion. TPLSM imaging revealed that while spontaneous or remote point stimulation-evoked $[Ca^{2+}]_i$ transients were observed to occur synchronously in host cardiomyocytes along the graft-host border, they were absent in all imaged BM-derived cell clusters, irrespective of the donor cell type. Electrical field stimulation was equally ineffective in triggering $[Ca^{2+}]_i$ transients in these cells. Together, our results indicate that the imaged donor-derived cells within the infarct scar are electrically inexcitable and/or unable to transiently raise cytosolic calcium in response to membrane depolarization. This result is consistent with the complete absence of sarcomeric alpha-actinin immune reactivity, and the presence of CD45 immune reactivity, in the EGFP-expressing donor-derived cells.

Our data also show that the TPLSM imaging system has limits with regards to axial resolution. Previous calculations have predicted that two-photon fluorescence excitation (and thus emission) in tissue is confined to less than femtoliter volumes around the focal point of a 1.2-numerical aperture water immersion objective, with <1 μm resolution in the *z* direction.[19,20,21] Wave front aberrations caused by the refractive index structure of the specimen have been known to compromise three-dimensional resolution in multiphoton laser scanning fluorescence microscopy.[22,23] Both theoretical and experimental approaches have shown that refractive index mismatch-induced optical aberrations cause a gradual decline primarily in axial resolution with increasing imaging depths into living biological, i.e. aqueous, specimens, even when water immersion objectives are used. In line with these observations, we found a significant axial broadening of the two-photon excitation volume with increasing distance of the focal plane from the epicardial surface of living, buffer-perfused mouse hearts, compromising the ability of our imaging system to properly discriminate donor cell-derived from host cell-derived rhod-2 signals within an axial distance of several microns from the donor-host interface. Our attempts to enhance the axial resolution by introducing a pinhole in the detection path resulted in near loss of the fluorescence signal at depth (data not shown), in accordance with previous reports.[24]

These physical constraints of the TPLSM imaging preclude its ability to discriminate the origin of rhod-2 fluorescence signals in small donor cells when they are closely juxtaposed to host

NIH-PA Author Manuscript

NIH-PA Author Manuscript

NIH-PA Author Manuscript

cardiomyocytes. Consequently, the system cannot be used to screen for the presence of functional attributes in isolated EGFP-expressing BM-derived cells that are located within a few microns from adjacent cardiomyocytes in the *z*-axis, given their small size. It is of interest to note that a TPLSM-based imaging approach was used in a recent study to demonstrate that some donor-derived cells apparently develop electrical stimulation-evoked rhod-2 transients in synchrony with host cardiomyocytes following engraftment into infarcted hearts.[16] However, control experiments demonstrating sufficient *in situ z*-axis spatial resolution to discriminate between signals originating in donor and host cells under the experimental conditions employed were lacking. Given the *z*-axis signal deterioration reported by us and others,[22,23] it is highly possible that the rhod-2 transients observed in donor-derived cells in that study arose as a consequence of fluorescence contamination from juxtaposed host cardiomyocytes, and does not represent intrinsic cardiomyogenic activity in the donor cell.

Collectively, our results are incompatible with previous studies suggesting that engrafted BM-derived cells exhibit both functional and structural characteristics of cardiomyocytes *in situ* (see Introduction). The underlying basis for this is not clear. Given the simplicity of isolation, it is unlikely that the LDM BM cells used here differed from those in studies which reported cardiomyogenic activity.[4,5] Similarly, flow cytometry analyses revealed that the scored attributes of the c-kit^{enr} BM cells and lin^{-} c-kit^{+} BM cells used here (Fig. 2 and Supplementary Fig. 1) appeared identical to those reported by others in studies reporting cardiomyogenic activity.[6,7] Thus it is unlikely that overt differences in the cellular composition of donor cell populations can explain the discrepancies in study outcome.

EGFP may selectively destroy a BM-derived cardiogenic precursor line, as previous studies revealed that the protein could be cytotoxic.[25,26] EGFP could also negatively interfere with cardiomyogenic activity. Finally, instability in EGFP fluorescent over time could give rise to a false negative result.[8] Several observations argue against these possibilities. First, the surface antigen expression profile in EGFP-expressing c-kit^{enr} BM cell population was identical with that in the entire, EGFP-positive and -negative, c-kit^{enr} population (see Supplementary Fig. 1). Second, adult *ACT-EGFP* cardiomyocytes stably express the fluorescent protein and function normally. Third, Orlic and co-workers [6] found that the percentage of engrafted BM-derived *bona fide* myocytes co-expressing EGFP and cardiomyocyte-specific markers was similar to that of EGFP-expressing c-kit-positive cells pre-transplantation, suggesting that EGFP does not negatively influence the transformation of BM cells into *bona fide* cardiomyocytes. Thus it is unlikely that the reporter gene negatively impacted cardiomyogenic activity in the current study.

On the other hand, our results are in excellent agreement with those of a number of previous studies that were conducted independently in different laboratories.[8,9,10,27] These studies exclusively relied on molecular analyses to follow BM cell fate following transplantation (see Introduction). In the present study, cross checking the results of functional and immunohistological analyses provided additional strong evidence that engrafted adult LDM BM cells, c-kit^{enr} BM cells, and lin^{-} c-kit^{+} BM cells do not give rise to high levels of functionally competent cardiomyocytes following direct injection into hearts of mice subjected to acute myocardial infarction. These data suggest that any functional improvement seen in infarcted hearts receiving BM cell transplants, both in animal studies and clinical trials, is likely to reflect a beneficial effect imparted upon the surviving, pre-existing myocardium, rather than a direct contribution of electromechanically integrated BM-derived *de-novo* cardiomyocytes. Possible mechanisms that underlie improvement in functional outcome following direct BM cell transplantation into ischemically injured myocardium appear to involve paracrine effects, resulting in prevention of cardiomyocyte apoptosis[28], preservation of cardiomyocyte function[28], and induction of angiogenesis[29,30].

NIH-PA Author Manuscript

NIH-PA Author Manuscript

NIH-PA Author Manuscript

Materials and Methods

All studies have been approved by the Institutional Review Board at the Indiana University School of Medicine.

Isolation of bone marrow cells for intracardiac transplantation

Bone marrow was obtained from the tibias, femurs, and iliac crests of 6-8-week-old heterozygous C57BL/6-Tg(ACTB-EGFP)1Osb/J mice of either sex (Jackson Laboratories, Bar Harbor, ME). This transgenic mouse line (designated *ACT-EGFP*) ubiquitously expresses enhanced green fluorescent protein (EGFP) under the control of the chicken β-actin promoter and cytomegalovirus enhancer. Three different subsets of BM cells were collected for intracardiac transplantation:

i) unfractionated low-density mononuclear BM (LDM) cells—The suspension of whole BM cells was overlaid with sodium metrizoate (Histopaque, Sigma, St. Louis, MI) solution (1.083 g/ml) and centrifuged at 740g for 25 min. The low-density cells were harvested, washed and suspended (100,000 cells in 3 μL PBS) in preparation for intracardiac injection.

ii) c-kit enriched (c-kit^{enr}) BM cells—LDM BM cells were reacted with a biotin-conjugated anti-mouse c-kit monoclonal antibody (clone ACK-4) and subsequently stained with streptavidin-phycoerythrin (SA-PE; Invitrogen Inc., Carlsbad, CA). The ACK-4/biotin/SA-PE – labeled cells were then incubated with anti-PE magnetic immunobeads (Miltenyi Biotec, Auburn, CA) and separated by magnet-activated cell sorting into c-kit^{+} and c-kit^{-} fractions. Cells expressing high levels of c-kit were used for intracardiac injection (c-kit^{enr} group).

iii) lineage-depleted BM cells expressing high numbers of c-kit receptors (lin^{-} c-kit^{+} cells)—LDM BM cells were incubated with a mixture of rat monoclonal antibodies directed against the following murine hematopoetic cell lineage –specific surface markers: B lymphocytes (B220), T lymphocytes (CD4 and CD8), granulocytes (Gr-1), myelomonocyic cells (Mac-1), and erythroid cells (Ter-119) (Pharmingen, San Diego, CA)[15]. Antibody-labeled lin^{+} cells were depleted using magnetic immunobeads (Miltenyi Biotec). The lineage-depleted cell population was then collected and incubated with a PE-conjugated anti-c-kit monoclonal antibody (clone ACK-4; Cedarlane Laboratories, Burlingtion, NC). Stained cells were sorted using a Becton-Dickonson cell sorter (Becton-Dickinson, Franklin Lakes, NJ) based on number of c-kit receptors and levels of EGFP expression. Lin^{-} cells expressing high levels of both c-kit and EGFP were used for intracardiac transplantation (lin^{-} c-kit^{+} group).

Flow cytometry analyses of c-kit^{enr} BM cells

In a separate set of experiments, we determined the expression levels of different markers on the surface of *ACT-EGFP* c-kit^{enr} BM cells using flow cytometry. c-kit^{enr} BM cells were collected from heterozygous *ACT-EGFP* mice as described above. Because eluted cells were already reacted with CD117 that was developed by a PE-conjugated second step reagent, aliquots of these cells were stained with other markers for analysis including PE-Cy5-conjugated sca-1, flk-1 APC, a cocktail of APC-conjugated lineage markers (CD3e, CD11b, CD45R/B220, Gr-1, and TER119), and biotinylated CD34 that was further developed with streptavidin-conjugated APC-Cy7. Each aliquot was subsequently analyzed by flow cytometry to determine expression levels of these surface markers in the c-kit^{enr} cell population.

Coronary artery ligation and intracardiac grafting

Ten- to twelve-week-old, non-transgenic C57BL/6 mice were endotracheally intubated and ventilated with a rodent ventilator (Harvard Apparatus, Holliston, MA). Anesthesia was

NIH-PA Author Manuscript

NIH-PA Author Manuscript

NIH-PA Author Manuscript

maintained with inhalational isoflurane. A thoracotomy was performed and an 8-0 polypropylene ligature was placed around the distal left anterior descending coronary artery as described previously.[10] One hundred thousand donor cells suspended in 3 μL PBS were injected into the anterior and posterior infarct border zones of the ischemic myocardium 3–5 h after coronary ligation. The chest was closed and the animals were weaned from the ventilator and extubated.

Imaging of intracellular calcium transients using TPLSM

Imaging of intracellular calcium ($[Ca^{2+}]_i$) transients in Langendorff-perfused hearts was performed as described previously.[11,12] All hearts were subjected to TPLSM imaging at 9 or 10 days after intracardiac delivery of BM cells. Calcium responses in donor-derived cells and host cardiomyocytes were monitored during spontaneous sinus rhythm, electrical point stimulation at a site remote from the graft, and electrical field stimulation. For a more detailed description of the imaging approach see Supplementary Information.

Immunohistochemistry

Hearts were harvested 9 days after intracardiac injection of BM cells, washed in PBS, immersed in fixation solution (1% para-formaldehyde and 1% cacodylic acid in PBS) for 48 hours at 2 to 4 °C, cryoprotected in 30% sucrose, and frozen in optimum cutting temperature compound. Ten-μm cryosections were obtained and stained for EGFP alone (rabbit anti-EGFP; Millipore, Billerica, MA) and developed with diaminobenzidine, or were stained with an anti-CD45 primary antibody (rat anti-CD45; Pharmingen), visualized with an Alexa555-conjugated secondary antibody (Invitrogen) in combination with a FITC-conjugated goat anti-GFP antibody (Novus Biologicals, Littleton, CO), and nuclear stained with 4,6-diamidino-2-phenylindol dihydrochloride (DAPI; Molecular Probes). Tissue α-actinin immunereactivity was detected by a mouse monoclonal antibody (Sigma) and visualized with a rhodamine-conjugated secondary antibody (Millipore). Hematoxylin & Eosin and Sirius Red/Fast Green stainings were performed as described previously.[31]

Supplementary Material

Refer to Web version on PubMed Central for supplementary material.

Acknowledgements

The study was supported by the National Institutes of Health and the American Heart Association.

References

1. Rubart M, Field LJ. Cardiac regeneration: repopulating the heart. Annu Rev Physiol 2006;68:29–49. [PubMed: 16460265]
2. Bittner RE, Schöfer C, Weipoltshammer K, Ivanova S, Streubel B, Hauser E, et al. Recruitment of bone-marrow-derived cells by skeletal and cardiac muscle in adult dystrophic mdx mice. Anat Embryol (Berl) 1999;199:391–396. [PubMed: 10221450]
3. Jackson KA, Majka SM, Wang H, Pocius J, Hartley CJ, Majesky MW, et al. Regeneration of ischemic cardiac muscle and vascular endothelium by adult stem cells. J Clin Invest 2001;107:1395–1402. [PubMed: 11390421]
4. Xaymardan M, Tang L, Zagreda L, Pallante B, Zheng J, Chazen JL, et al. Platelet-derived growth factor-AB promotes the generation of adult bone marrow-derived cardiac myocytes. Circ Res 2004;94:E39–E45. [PubMed: 14963008]
5. Fernández-Avilés F, San Román JA, García-Frade J, Fernández ME, Peñarrubia MJ, de la Fuente L, et al. Experimental and clinical regenerative capability of human bone marrow cells after myocardial infarction. Circ Res 2004;95:742–748. [PubMed: 15358665]

NIH-PA Author Manuscript

NIH-PA Author Manuscript

NIH-PA Author Manuscript

6. Orlic D, Kajstura J, Chimenti S, Jakoniuk I, Anderson SM, Li B, Pickel J, et al. Bone marrow cells regenerate infarcted myocardium. Nature 2001;410:701–705. [PubMed: 11287958]
7. Kajstura J, Rota M, Whang B, Cascapera S, Hosoda T, Bearzi C. Bone marrow cells differentiate in cardiac cell lineages after infarction independently of cell fusion. Circ Res 2005;96:127–137. [PubMed: 15569828]
8. Balsam LB, Wagers AJ, Christensen JL, Kofidis T, Weissman IL, Robbins RC. Haematopoietic stem cells adopt mature haematopoietic fates in ischaemic myocardium. Nature 2004;428:668–673. [PubMed: 15034594]
9. Nygren JM, Jovinge S, Breitbach M, Säwén P, Röll W, Hescheler J, et al. Bone marrow-derived hematopoietic cells generate cardiomyocytes at a low frequency through cell fusion, but not transdifferentiation. Nat Med 2004;10:494–501. [PubMed: 15107841]
10. Murry CE, Soonpaa MH, Reinecke H, Nakajima H, Nakajima HO, Rubart M, et al. Haematopoietic stem cells do not transdifferentiate into cardiac myocytes in myocardial infarcts. Nature 2004;428:664–668. [PubMed: 15034593]
11. Rubart M, Wang E, Dunn KW, Field LJ. Two-photon molecular excitation imaging of Ca^{2+} transients in Langendorff-perfused mouse hearts. Am J Physiol Cell Physiol 2003;284:C1654–C1568. [PubMed: 12584115]
12. Rubart M, Pasumarthi KB, Nakajima H, Soonpaa MH, Nakajima HO, Field LJ. Physiological coupling of donor and host cardiomyocytes after cellular transplantation. Circ Res 2003;92:1217–1224. [PubMed: 12730096]
13. Okabe M, Ikawa M, Kominami K, Nakanishi T, Nishimune Y. 'Green mice' as a source of ubiquitous green cells. FEBS Lett 1997;407:313–319. [PubMed: 9175875]
14. Orlic D, Kajstura J, Chimenti S, Bodine DM, Leri A, Anversa P. Transplanted adult bone marrow cells repair myocardial infarcts in mice. Ann N Y Acad Sci 2001;938:221–229. [PubMed: 11458511]
15. Orlic D, Fischer R, Nishikawa S, Nienhuis AW, Bodine DM. Purification and characterization of heterogeneous pluripotent hematopoietic stem cell populations expressing high levels of c-kit receptor. Blood 1993;82:762–770. [PubMed: 7687891]
16. Rota M, Kajstura J, Hosoda T, Bearzi C, Vitale S, Esposito G, et al. Bone marrow cells adopt the cardiomyogenic fate in vivo. Proc Natl Acad Sci U S A 2007;104:17783–17788. [PubMed: 17965233]
17. Laflamme MA, Murry CE. Regenerating the heart. Nat Biotechnol 2005;23:845–856. [PubMed: 16003373]
18. Haudek SB, Xia Y, Huebener P, Lee JM, Carlson S, Crawford JR, et al. Bone marrow-derived fibroblast precursors mediate ischemic cardiomyopathy in mice. Proc Natl Acad Sci U S A 2006;103:18284–18289. [PubMed: 17114286]
19. Rubart M. Two-photon microscopy of cells and tissue. Circ Res 2004;95:1154–1166. [PubMed: 15591237]
20. Helmchen F, Svoboda K, Denk W, Tank DW. In vivo dendritic calcium dynamics in deep-layer cortical pyramidal neurons. Nat Neurosci 1999;2:989–996. [PubMed: 10526338]
21. Brown EB, Shear JB, Adams SR, Tsien RY, Webb WW. Photolysis of caged calcium in femtoliter volumes using two-photon excitation. Biophys J 1999;76:489–499. [PubMed: 9876162]
22. Booth MJ, Wilson T. Refractive-index-mismatch induced aberrations in single-photon and two-photon microscopy and the use of aberration correction. J Biomedical Optics 2001;6:266–272.
23. Niesner R, Andresen V, Neumann J, Spiecker H, Gunzer M. The power of single and multibeam two-photon microscopy for high-resolution and high-speed deep tissue and intravital imaging. Biophys J 2007;93:2519–2529. [PubMed: 17557785]
24. Gauderon R, Lukins PB, Sheppard CJ. Effect of a confocal pinhole in two-photon microscopy. Microsc Res Tech 1999;47:210–214. [PubMed: 10544336]
25. Huang WY, Aramburu J, Douglas PS, Izumo S. Transgenic expression of green fluorescence protein can cause dilated cardiomyopathy. Nat Med 2000;6:482–483. [PubMed: 10802676]
26. Agbulut O, Coirault C, Niederländer N, Huet A, Vicart P, Hagège A, et al. GFP expression in muscle cells impairs actin-myosin interactions: implications for cell therapy. Nat Meth 2006;3:331.
27. Deten A, Volz HC, Clamors S, Leiblein S, Briest W, Marx G, et al. Hematopoietic stem cells do not repair the infarcted mouse heart. Cardiovasc Res 2005;65:52–63. [PubMed: 15621033]

NIH-PA Author Manuscript

NIH-PA Author Manuscript

NIH-PA Author Manuscript

28. Uemura R, Xu M, Ahmad N, Ashraf M. Bone marrow stem cells prevent left ventricular remodeling of ischemic heart through paracrine signaling. Circ Res 2006;98:1414–1421. [PubMed: 16690882]

29. Kamihata H, Matsubara H, Nishiue T, Fujiyama S, Tsutsumi Y, Ozono R, et al. Implantation of bone marrow mononuclear cells into ischemic myocardium enhances collateral perfusion and regional function via side supply of angioblasts, angiogenic ligands, and cytokines. Circulation 2001;104:1046–1052. [PubMed: 11524400]

30. Fazel S, Cimini M, Chen L, Li S, Angoulvant D, Fedak P, et al. Cardioprotective c-kit^{+} cells are from the bone marrow and regulate the myocardial balance of angiogenic cytokines. J Clin Invest 2006;116:1865–1877. [PubMed: 16823487]

31. Nakajima H, Nakajima HO, Dembowsky K, Pasumarthi KB, Field LJ. Cardiomyocyte cell cycle activation ameliorates fibrosis in the atrium. Circ Res 2006;98:141–148. [PubMed: 16306446]

NIH-PA Author Manuscript
NIH-PA Author Manuscript
NIH-PA Author Manuscript

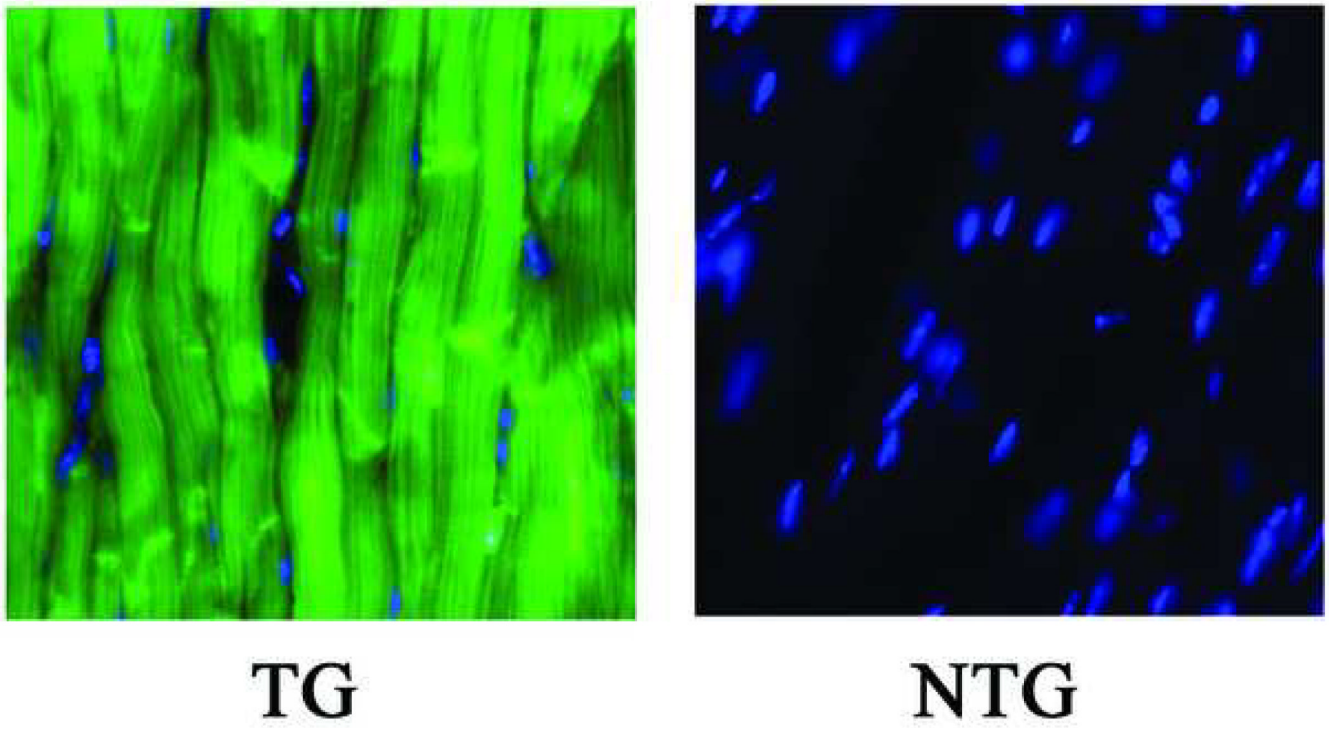

Figure 1.
Representative epifluorescence images of 10-μm sections obtained from adult hearts of an *ACT-EGFP* transgenic (TG) mouse and its non-transgenic (NTG) littermate. Sections were stained with Hoechst. Images for EGFP (green) and Hoechst (blue) fluorescence were merged. Imaging parameters were identical for both sections.

NIH-PA Author Manuscript
NIH-PA Author Manuscript
NIH-PA Author Manuscript

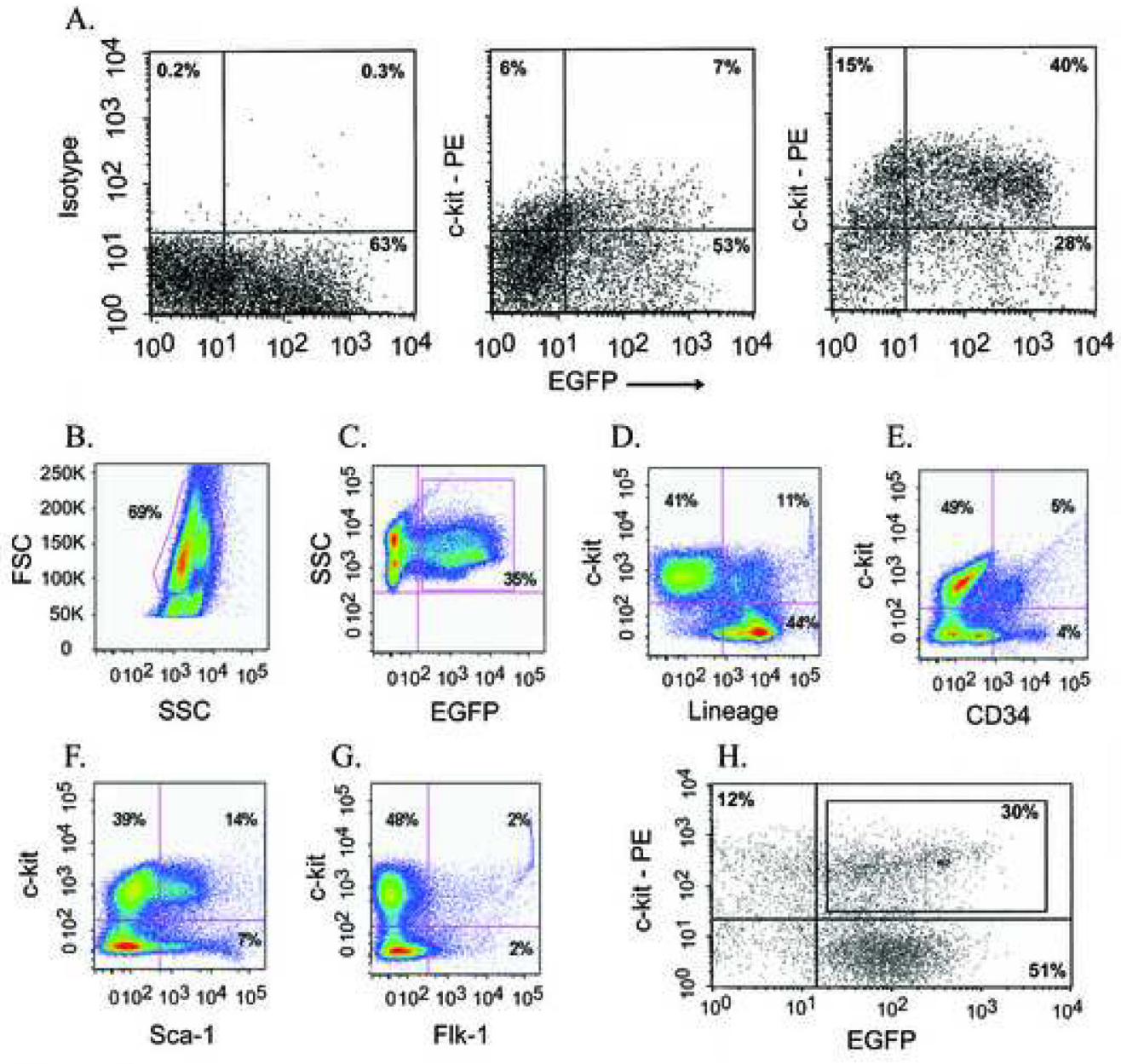

Figure 2.

Analysis of c-kit^{enr} (panels **A–G**) and highly enriched lin^{-} c-kit^{+} (panel **H**) BM cells. (**A**) Representative flow cytometry dot plots of the eluted (positively labeled; right panel) and eluent (unlabeled; middle panel) fraction of c-kit^{enr} BM cells based on levels of EGFP (X axis) and c-kit (Y axis) expression. Left panel shows isotype control. Axes are log-scaled. (**B – G**) Flow cytometry analyses of surface antigen expression in *ACT-EGFP* c-kit^{enr} BM cells. c-kit^{enr} BM cells were selected for c-kit^{+} (CD117^{+}) cells using MACS as described in Materials and Methods. (**B**) Light scatter gating of eluted cells identified approximately 70 % of the cells within the low density mononuclear gate (FSC, forward scatter). (**C**) Analysis of GFP expression versus side scatter (SSC) identified 35 % of eluted cells as GFP^{+}. (**D**) Expression of lineage markers (X axis) versus c-kit expression (Y axis) among cells falling within the

NIH-PA Author Manuscript

NIH-PA Author Manuscript

NIH-PA Author Manuscript

mononuclear gate as defined in panel B. (**E**) Expression of CD34 (X axis) versus c-kit expression (Y axis) among cells falling within the lymphocyte gate. (**F**) Expression of Sca-1 (X axis) versus c-kit expression (Y axis) among cells falling within the mononuclear gate. (**G**) Expression of Flk-1 (X axis) versus c-kit expression (Y axis) among cells falling within the mononuclear gate. (**H**) Fluorescence-activated cell sorting (FACS) of *ACT-EGFP*, lineage-depleted (lin^-) mouse BM cells based on c-kit- and EGFP-expression. Representative FACS dot plot of lin^- BM cells stained with ACK-4/Biotin/SA-PE. Antibody-labeled cells were separated by FACS into four subsets based on number of c-kit receptors (Y axis) and levels of EGFP (X axis) expression. Box in upper right rectangle indicates fraction of $c\text{-}kit^+/EGFP^+$ cells that was used for cell transplantation (lin^- $c\text{-}kit^+$ group). Mean expression levels of both c-kit and EGFP in $c\text{-}kit^+/EGFP^+$ cells were ~ 2-fold to ~ 100-fold higher than those in $c\text{-}kit^-/EGFP^-$ cells (lower left rectangle).

NIH-PA Author Manuscript
NIH-PA Author Manuscript
NIH-PA Author Manuscript

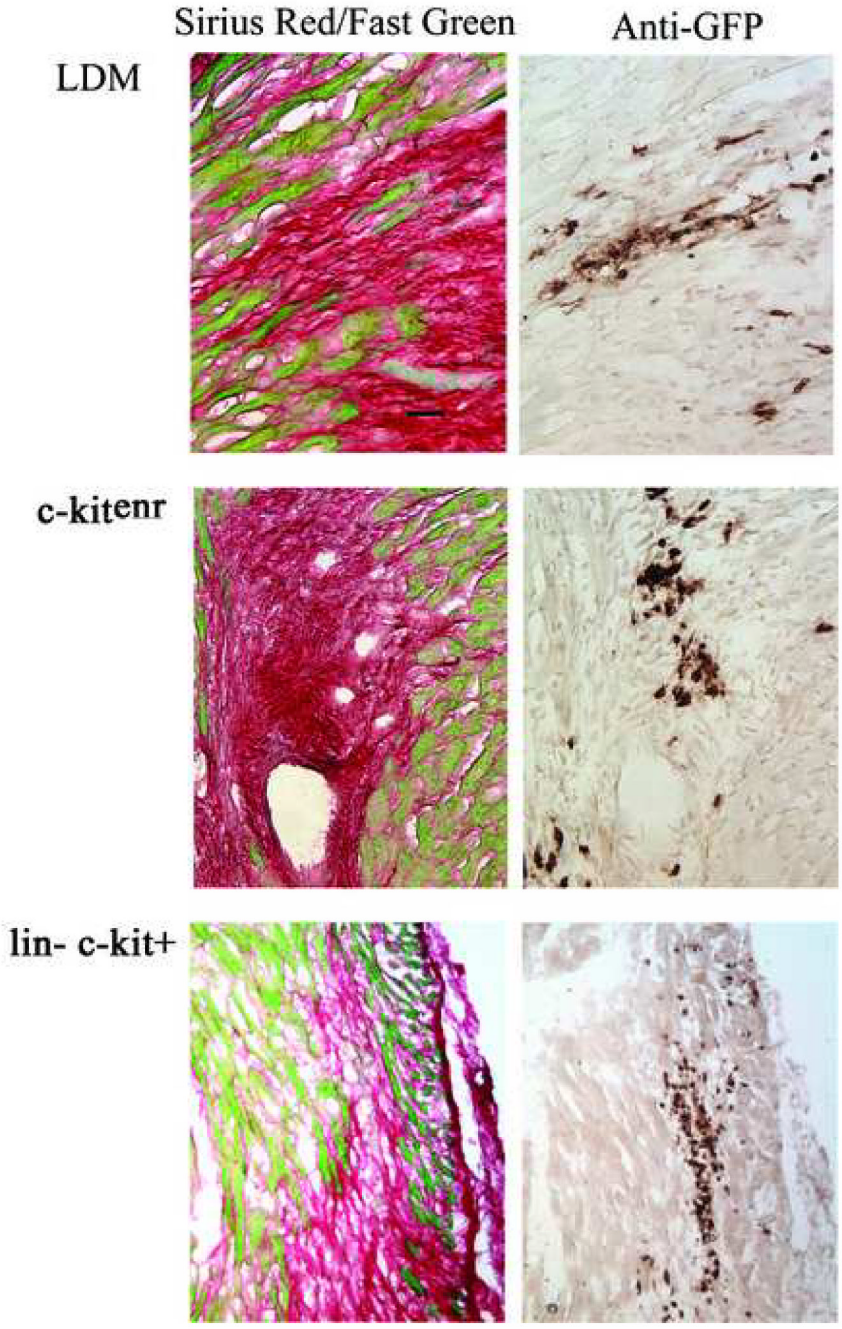

Figure 3.

Direct transplantation and engraftment of *ACT-EGFP* BM cells into infarcted myocardium of non-transgenic recipients. Left panels: Sirius Red and Fast Green stained histological sections from infarcted hearts at 9 days following left coronary artery ligation and transplantation of 100,000 *ACT-EGFP* BM cells. Right panels: adjacent sections from the same hearts immunostained for EGFP (brown signal, HRP-conjugated secondary antibody, signal developed with diaminobezidine reaction). Scale bar: 30 μm.

NIH-PA Author Manuscript
NIH-PA Author Manuscript
NIH-PA Author Manuscript

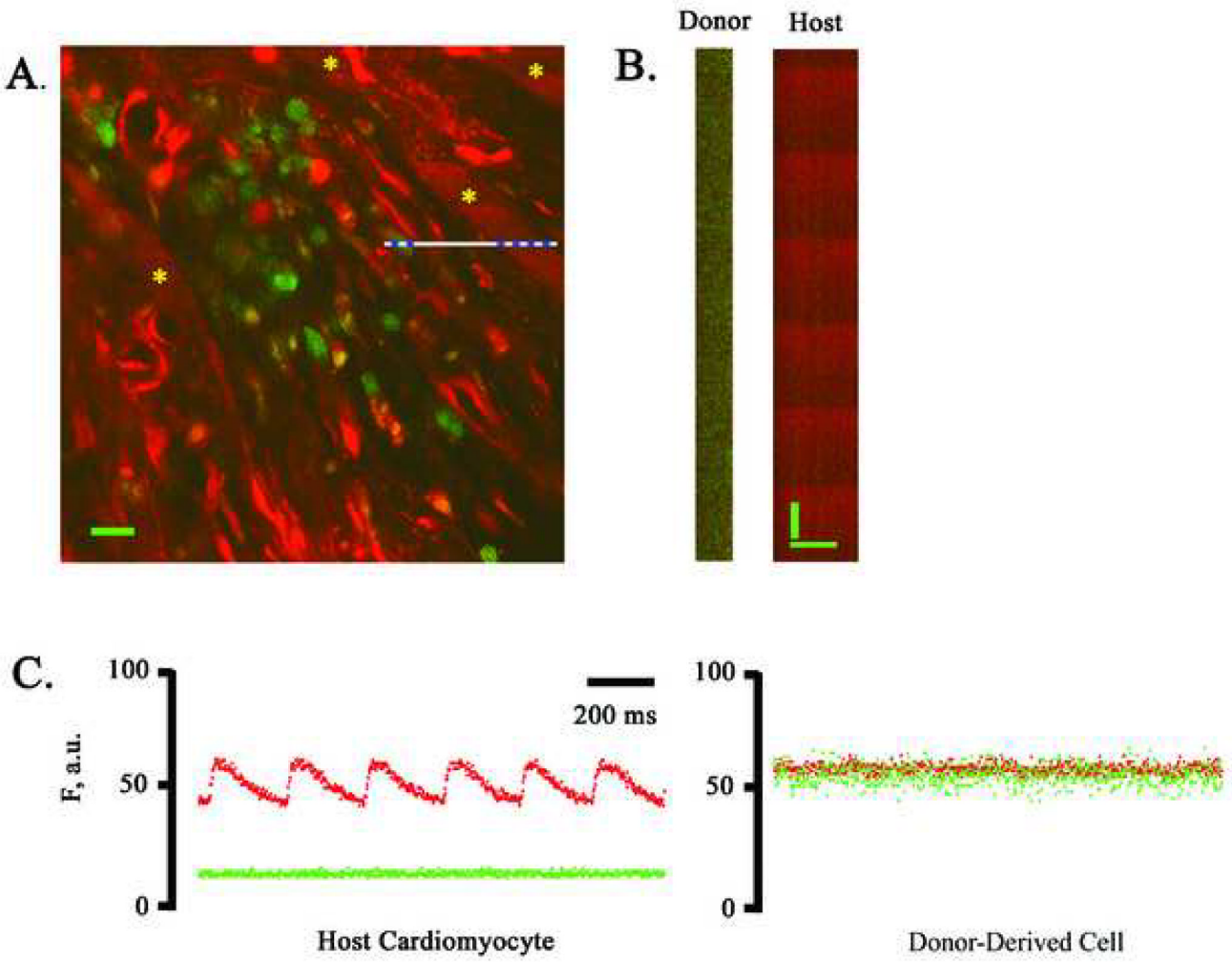

Figure 4.

Simultaneous imaging of rhod-2 and EGFP fluorescence in a non-transgenic heart at 9 days following coronary artery ligation and injection of *ACT-EGFP* LDM BM cells into the peri-infarct zone. (**A**) Full-frame TPLSM image of the graft/host myocardium border zone. Hearts were loaded with rhod-2. Red (rhod-2) and green (EGFP) fluorescence signals were superimposed. Host cardiomyocytes and donor-derived cells (green/yellow) are apparent. The preparation was paced via point stimulation at a remote site at 4 Hz. The white bar demarks the position of line-scan mode data acquisition. Asterisks mark host cardiomyocytes with $[Ca^{2+}]_i$ transients. Scale bar: 20 μm. (**B**) Stacked line-scan images of the regions in panel A demarked by the blue dotted lines. Line-scans traverse one non-EGFP-expressing, i.e. host, cardiomyocyte and one EGFP-expressing, i.e. donor-derived, cell. Scale bars: 20 μm horizontally, 125 ms vertically. (**C**) Spatially integrated changes in rhod-2 and EGFP fluorescence for one host cardiomyocyte and one juxtaposed donor-derived cell. The fluorescence signal across the entire cell was averaged. F, fluorescence; a.u., arbitrary units. (**D**) Full-frame TPLSM images obtained from the heart depicted in **A** at increasing depth. The heart was paced via point stimulation at a remote site at 4 Hz. Numbers indicate nominal distance of focal plane from the epicardial surface. Scale bar: 20 μm.

NIH-PA Author Manuscript
NIH-PA Author Manuscript
NIH-PA Author Manuscript

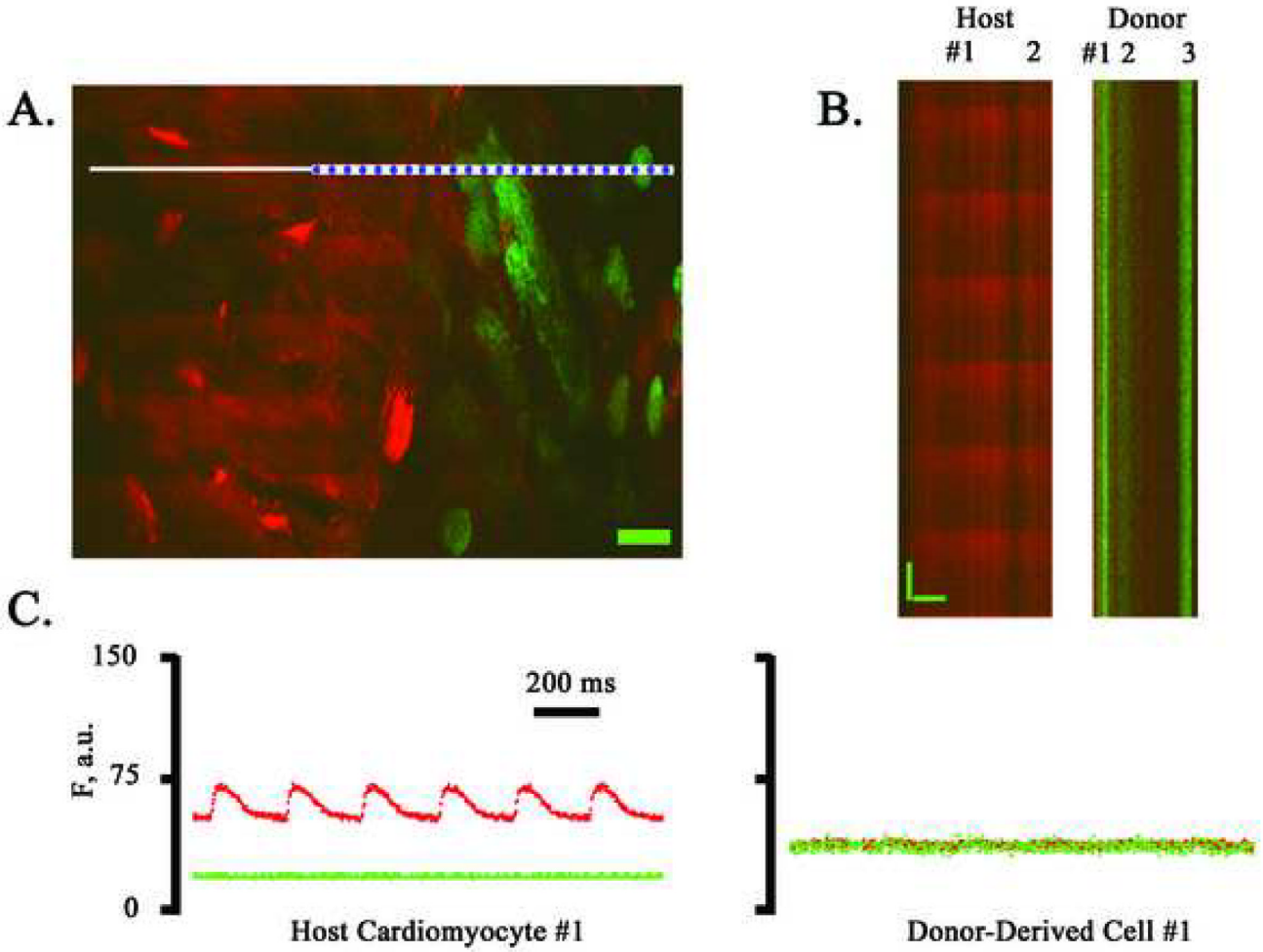

Figure 5.

Simultaneous imaging of rhod-2 and EGFP fluorescence in a non-transgenic heart at 9 days following coronary artery ligation and injection of *ACT-EGFP* c-kit^{enr} BM cells into the peri-infarct zone. **A**, Full-frame TPLSM image of the graft/host myocardium border zone. Hearts were loaded with rhod-2. Host cardiomyocytes (red) and donor-derived cells (green/yellow) are apparent. The preparation was paced via point stimulation at a remote site at 4 Hz. The white bar demarks the position of line-scan mode data acquisition. Scale bar: 20 μm. (**B**) Stacked line-scan images of the regions in panel A demarked by the blue dotted lines. Line-scans traverse two non-EGFP-expressing, i.e. host, cardiomyocytes and three EGFP-expressing, i.e. donor-derived, cells. Scale bars: 20 μm horizontally, 125 ms vertically. (**C**) Spatially integrated changes in rhod-2 and EGFP fluorescence for one host cardiomyocyte and one juxtaposed donor-derived cell. The fluorescence signal across the entire cell was averaged. F, fluorescence; a.u., arbitrary units.

NIH-PA Author Manuscript
NIH-PA Author Manuscript
NIH-PA Author Manuscript

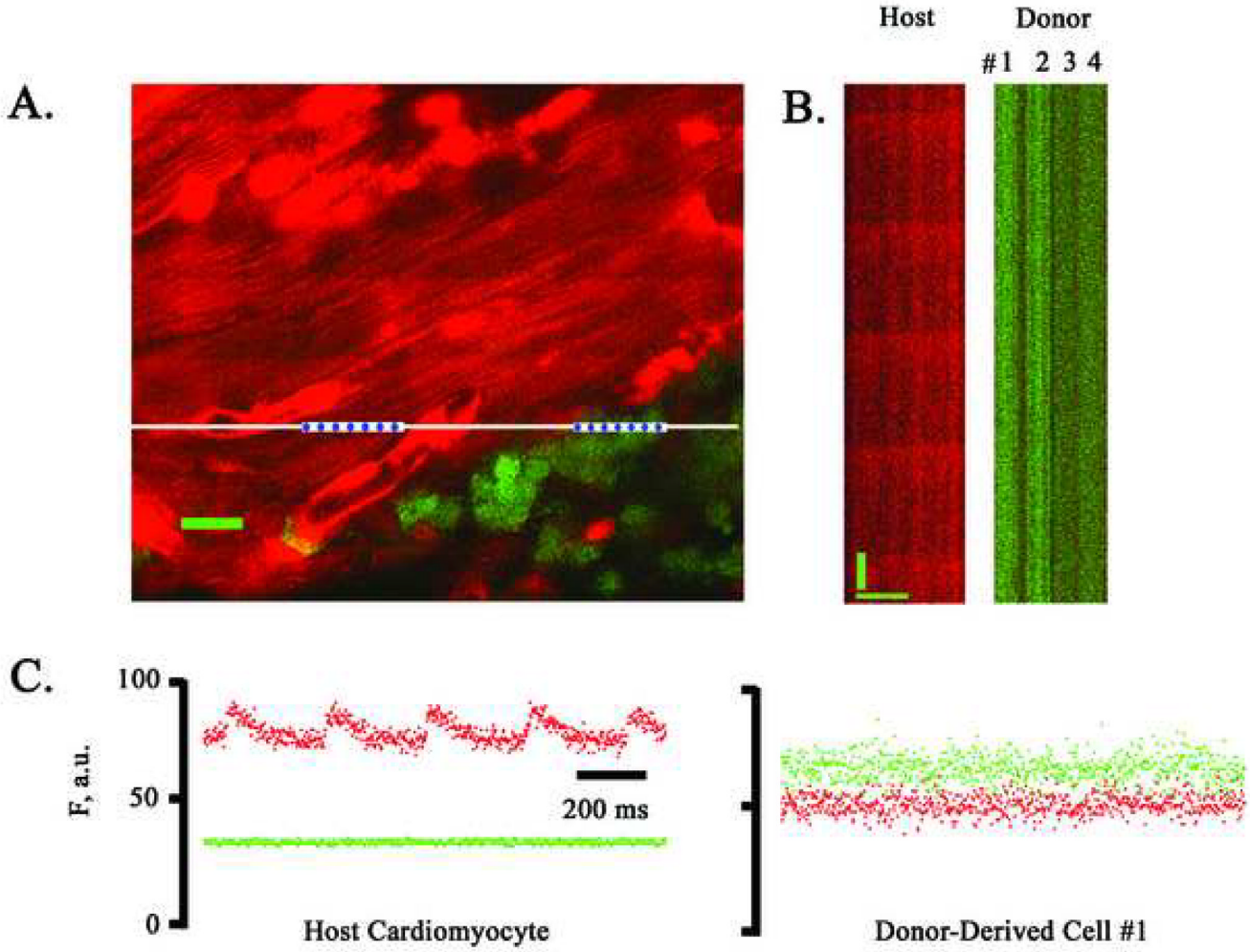

Figure 6.

Simultaneous imaging of rhod-2 and EGFP fluorescence in a non-transgenic heart at 9 days following coronary artery ligation and injection of *ACT-EGFP* lin$^-$ c-kit$^+$ BM cells into the peri-infarct zone. (**A**) Full-frame TPLSM image of the rhod-2 loaded heart at the graft-host border zone. The heart was continuously paced via point stimulation at a remote site at 3 Hz. Red (rhod-2) and green (EGFP) fluorescence signals were superimposed. Host cardiomyocytes (red) and donor-derived cells (green/yellow) are apparent. White line demarks the position of line-scan mode data acquisition. Scale bar: 20 μm. (**B**) Line-scan mode images of the regions in panel A demarked by the blue dotted lines. The line scans traverse one EGFP-negative (i.e. host) cardiomyocyte and four EGFP-expressing (i.e. donor-derived) cells. Scale bars: 20 μm horizontally, 125 ms vertically. (**C**) Spatially integrated changes in rhod-2 and EGFP fluorescence for one host cardiomyocyte and one donor-derived cell. The fluorescence signal across the entire cell was averaged. F, fluorescence; a.u., arbitrary units.

NIH-PA Author Manuscript
NIH-PA Author Manuscript
NIH-PA Author Manuscript

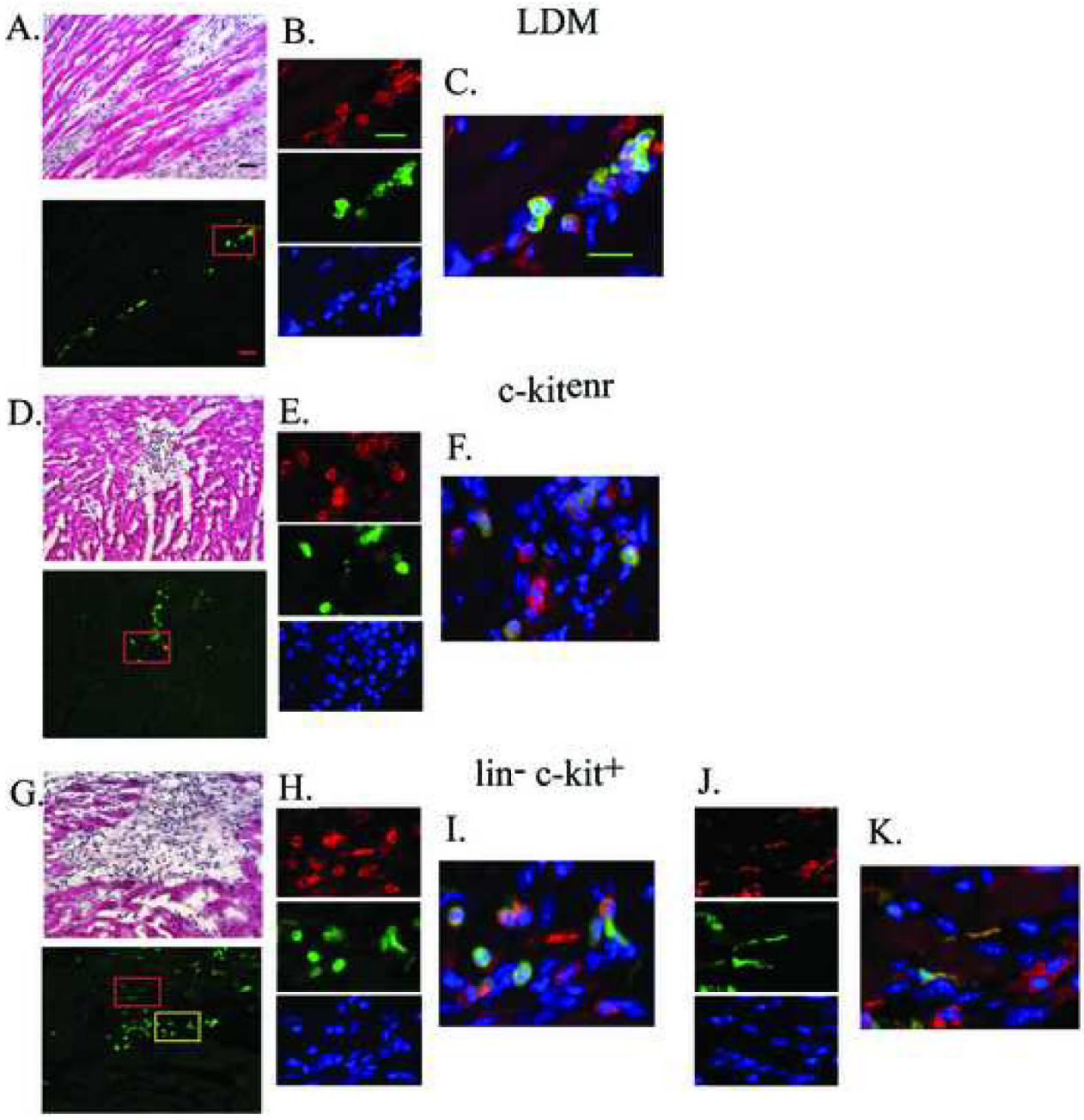

Figure 7.

Immune histological analyses for CD45, EGFP and α-actinin in 10-μm sections obtained from non-transgenic hearts at 9 days following coronary artery ligation and *ACT-EGFP* LDM (**A–C**), c-kit^{enr} (**D–F**) or lin^{-} c-kit^{+} (**G–K**) BM cells. The upper panels in A, D and G show representative Hematoxylin and Eosin (H&E)-stained sections of the transition zone between the surviving host myocardium and the infarct scar in the engrafted hearts. The lower panels show that the donor-derived cells (green) predominately engraft within scar tissue or at the infarct border zone, rather than within viable myocardium. The upper panels in B, E, H and J show representative images of CD45 expression, the middle panels show EGFP expression, and the lower panels show Hoechst nuclear staining; data is taken from the regions boxed in

NIH-PA Author Manuscript

NIH-PA Author Manuscript

NIH-PA Author Manuscript

panels A, D and G (panels H and J correspond to the yellow and red box, respectively, in panel G). Panels C, F, I and K show the corresponding merged fluorescence images. Scale bar 30 μm in A; 20 μm in B and C. (**L**) α-actinin (red) expression, EGFP (green) expression and Hoechst nuclear staining in tissue sections adjacent to those shown in A, D and G. Scale bar, 20 μm.

NIH-PA Author Manuscript
NIH-PA Author Manuscript
NIH-PA Author Manuscript

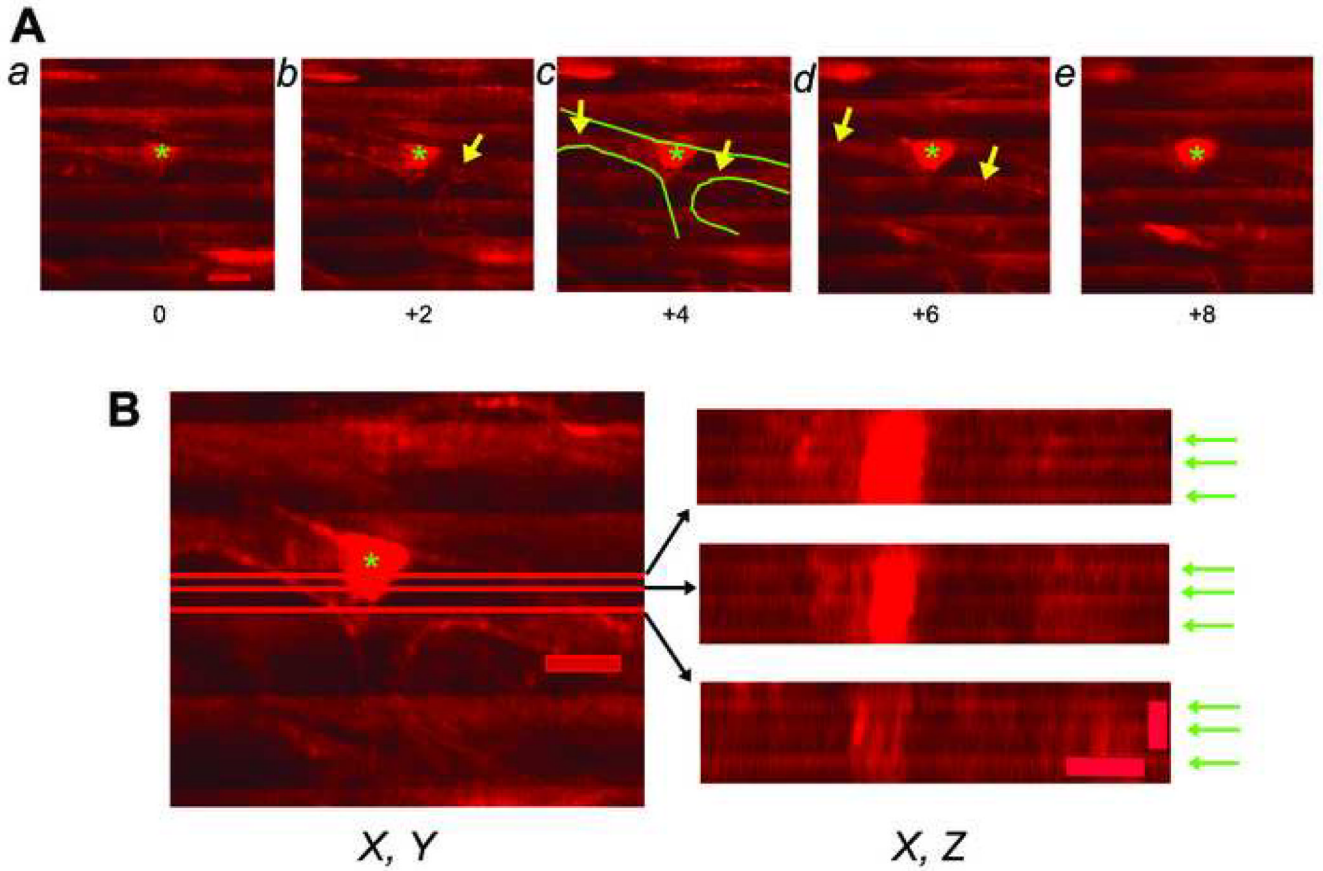

Figure 8.

Spatial resolution of the imaging system in living heart tissue. (**A**) Series of *X, Y* scans obtained from an isolated perfused mouse heart loaded with rhod-2 using TPLSM in non-descanned mode. Images were collected across a bifurcating capillary at 2-μm *z*-steps intervals during continuous electrical point stimulation at 4 Hz. Numbers indicate imaging depth (in μm) in reference to the image in panel *a*. The wave length of excitation light was 810 nm and rhod-2 fluorescence was collected between 560 nm and 650 nm. Green lines in panel *c* mark the capillary endothelium. Asterisks denote endothelial cell nuclei. Periodic increases in rhod-2 fluorescence resulting from action potential–evoked increases in cytosolic calcium concentration are visible as ripple-like wave fronts. Some *X, Y* scans reveal the appearance of cardiomyocyte-typical rhod-2 transients within the perfusate-filled capillary lumen (arrows). Scale bar, 10 μm. (**B**) Data sets shown in A were converted to a stack, and the stack was then resliced to obtain *X, Z* projections of the capillary. Red lines in the *X, Y* scan on the left indicate the *X* positions of the *X, Z* profiles shown on the right. Green arrows denote action potential-induced rhod-2 transients. In all three projections, rhod-2 transients are clearly detectable within the capillary lumen. Scale bars: 10 μm laterally, 5 μm axially.